Atmos. Chem. Phys., 24, 993–1003, 2024
https://doi.org/10.5194/acp-24-993-2024

Atmospheric Chemistry and Physics
Open Access
EGU

A study on the influence of inorganic ions, organic carbon and microstructure on the hygroscopic property of soot

Zhanyu Su[1,2], Lanxiadi Chen[2,3], Yuan Liu[1,2], Peng Zhang[1], Tianzeng Chen[1], Biwu Chu[1,2], Mingjin Tang[2,3], Qingxin Ma[1,2], and Hong He[1,2]

[1]State Key Joint Laboratory of Environment Simulation and Pollution Control, Research Center for Eco-Environmental Sciences, Chinese Academy of Sciences, Beijing 100085, China
[2]College of Resources and Environment, University of Chinese Academy of Sciences, Beijing 100049, China
[3]State Key Laboratory of Organic Geochemistry, Guangzhou Institute of Geochemistry, Chinese Academy of Sciences, Guangdong 510640, China

Correspondence: Qingxin Ma (qxma@rcees.ac.cn)

Received: 17 August 2023 – Discussion started: 30 August 2023
Revised: 27 November 2023 – Accepted: 3 December 2023 – Published: 23 January 2024

Abstract. Soot is a crucial component of aerosols in the atmosphere. Understanding the hygroscopicity of soot particles is important for studying their role as cloud condensation nuclei (CCN) as well as their chemical behavior and atmospheric lifetime. However, there is still a lack of comprehensive understanding regarding the factors that determine the hygroscopic properties of soot. In this work, the hygroscopic behavior of soot particles generated from different types of fuel combustion and aged with SO_2 for varying durations was measured by a vapor sorption analyzer. Various characterizations of soot were conducted to understand the key factors that influence the hygroscopic properties of soot. It was found that water-soluble substances in soot facilitate the completion of monolayer water adsorption at low relative humidity and increase the number of water adsorption layers at high relative humidity. On the other hand, soot prepared from fuel burning typically lacks water-soluble inorganic ions, and their hygroscopicity is primarily influenced by organic carbon (OC) and microstructure. Furthermore, the hygroscopicity of soot can be enhanced by the formation of sulfate due to heterogeneous oxidation of SO_2. These finding sheds light on the critical factors that affect soot hygroscopicity during water adsorption and allows for estimating the interaction between water molecules and soot particles in a humid atmosphere.

1 Introduction

Soot particles are produced by incomplete combustion processes of carbon-containing materials (Petzold et al., 2013). The current global emission of soot has been estimated to be 3–8 TgC yr^{-1} (Forster et al., 2007). Soot aerosol can influence climate by directly absorbing solar radiation and affecting cloud formation and surface albedo through deposition on snow and ice (Liao et al., 2015; Peng et al., 2016), which results in a contribution of soot to anthropogenic radiative forcing second only to that of CO_2 (Bond et al., 2013; Cappa et al., 2012; Liu et al., 2017). In addition, soot particles can significantly enhance the atmospheric oxidation capacity (He et al., 2022) and contribute to the formation of secondary aerosols by providing an active surface for the heterogeneous reactions of gaseous pollutants like NO_2, SO_2 and volatile organic compounds (VOCs) (Tritscher et al., 2011; Han et al., 2017; Zhang et al., 2022b; Liu et al., 2023). Moreover, soot particles also pose a health risk by causing and enhancing respiratory, cardiovascular and allergic diseases (Janssen et al., 2011; Lin et al., 2011). Due to its significant effect on global climate change, regional air quality and human health, the physicochemical properties of soot have attracted much attention in recent decades.

Hygroscopicity is one of the most important physicochemical properties of soot, which largely determines the cloud condensation nuclei (CCN) activity as well as the consequent radiation forcing (Semeniuk et al., 2007; Ramanathan and Carmichael, 2008; Friedman et al., 2011). On the other hand, the hygroscopicity of atmospheric particles is important for their chemical behavior because water molecules were found to significantly affect the heterogeneous transformation of gaseous pollutants on soot surfaces (Zhao et al., 2017; He and He, 2020; Zhang et al., 2022b).

The hygroscopic behavior of soot has been widely studied. It was found that soot prepared in laboratory or commercial soot appears to be hydrophobic as there is no noticeable uptake of water at unsaturated humidity. For instance, the commercial soot and spark discharge soot particles shrunk with increasing relative humidity (RH) during the growth factor measurements by hygroscopicity tandem differential mobility analyzers (H-TDMA) (Weingartner et al., 1997; Henning et al., 2010). This was explained with a restructuring of the agglomerated particles. Due to the inverse Kelvin effect, water condenses in small angle cavities of soot particles, which leads to capillary forces on the branches of the aggregates and causes them to collapse. Different from the commercial soot and spark discharge soot, diesel soot, aircraft soot and biomass smoke particles showed obvious particle size growth with increasing RH (Popovicheva et al., 2008; Carrico et al., 2010). This indicates that the chemical composition of soot is an important factor affecting its hygroscopicity. Our previous study suggested that combustion conditions could affect the morphology and microstructure of soot, which has a significant effect on the hygroscopicity (Han et al., 2012).

Soot aerosols experience internal mixing with other compounds (inorganic, organic or inorganic–organic mixtures) as aging after their emission (Shiraiwa et al., 2007; Matsui et al., 2013). Field observations have demonstrated that the presence of BC-coating materials greatly influences both the hygroscopic properties and the CCN properties (or the wet removal) (Ohata et al., 2016; Li et al., 2018; Hu et al., 2021). Several laboratory studies have also simulated the hygroscopic changes in soot particles during atmospheric transport and aging. Soot particles generated from incomplete combustion of propane were exposed to the oxidation products of the OH-toluene reaction, resulting in an organic coating that increased the hygroscopicity of the particles (Qiu et al., 2012). Moreover, the aging process of propane flame soot through NO_2 oxidation of SO_2 was found to produce inorganic hydrophilic coating materials and significantly enhance the CCN activity of soot particles (Zhang et al., 2022a).

The hygroscopicity of soot can vary significantly depending on its source and aging processes, which has implications for regional air quality and climate. However, previous studies have often focused on specific factors influencing the hygroscopicity of a particular type of soot, lacking a comprehensive understanding of the key factors determining the hygroscopic properties of soot. In this study, we conducted measurements to determine the hygroscopicity of soot produced from different fuels and aged with SO_2 for different times. In addition, the chemical composition and microstructure of soot were characterized for each soot sample. The main objectives of this study were to compare the hygroscopicity of soot from different sources and analyze the effect of organic carbon (OC), water-soluble ions and microstructure on the multilayer adsorption of soot surface water. Moreover, the impact of heterogeneous aging reactions on the multilayer adsorption of water on the surface of soot particles was also explored. This study contributes to a deeper understanding of the hygroscopicity and atmospheric impacts of soot particles in the atmosphere.

2 Experimental section

2.1 Soot samples

Prepared soot particles were obtained by burning *n*-hexane, decane or toluene (AR, Sinopharm Chemical Reagent Lo., Ltd) in a co-flow system as described in our previous studies (Han et al., 2012; Zhao et al., 2017). Briefly, the co-flow burner consisted of a diffusion flame maintained in a flow of synthetic air. Soot was collected on a quartz disk (7 cm in diameter) over a diffusion flame and then stored in a brown bottle (Agilent). Diesel soot (DS) was collected from the diesel particle filter (DPF) of a China VI heavy-duty diesel engine (ISUZU from China). A diesel engine bench test was run under the conditions of the World Harmonized Transient Cycle (WHTC). China VI fuels were used in the study, meeting the GB T32859-2016 standard. Printex U powder (U-soot) from Degussa (CAS no.: 1333-86-4) was used as model soot. These types of soot are usually used in laboratory simulations as representative of soot in the atmosphere (Liu et al., 2010; Han et al., 2012; Zhang et al., 2022b).

The aging experiments were performed in a quartz flow tube reactor. Prior to the reaction, the 0.05 g U-soot powder was placed into the quartz flow tube reactor. The experiments were maintained at 25 °C. Zero air was used as the carrier gas with a total flow rate about 700 mL min^{-1}. The SO_2 concentration was 5 ppm. The relative humidity (RH) of the aging reaction was 50 % RH (recorded with Vaisala HMP110). To simulate solar irradiation, a high-uniformity integrated xenon lamp (PLS-FX300HU, Beijing Perfectlight Technology Co., Ltd.) of 270 mW cm^{-2} was used as the light source. Its visible spectrum ranges from 330 to 850 nm.

2.2 Characterization of soot

A transmission electron microscope (H-7500, Hitachi) was used to investigate the morphologies of soot particles. The DS sample was ultrasonically dispersed in ethanol, while other soot samples were ultrasonically dispersed in ultrapure water (18.2 MΩ cm). Then, a droplet of suspension was deposited onto a Cu microgrid. An acceleration voltage of

200 kV was used for measurements. The diameter of particles was analyzed by ImageJ 1.41 software.

Raman spectra of soots were obtained with a Renishaw inVia Raman microscope system using a 532 nm excitation wavelength. The exposure time for each scan was 60 s. Data were acquired and analyzed using the Renishaw WiRE 5.4 software.

The content of OC was measured using a thermal–optical transmittance OC/EC (elemental carbon) analyzer (Sunset laboratory Inc., Forest Grove, OR) with a modified NIOSH 5040 protocol, and this produced four OC fractions (OC1, OC2, OC3 and OC4 at 150, 250, 450 and 550 °C, respectively), an OP (pyrolyzed organic) fraction (a pyrolyzed carbonaceous component determined when the transmitted laser returned to its original intensity after the sample was exposed to oxygen), and three EC fractions (EC1, EC2 and EC3 at 550, 700 and 800 °C, respectively). OC is defined as OC1 + OC2 + OC3 + OC4 + OP and EC is defined as EC1 + EC2 + EC3-OP (Chow et al., 1993; Li et al., 2016).

The chemical compositions of OC in soots were identified via gas chromatography coupled with mass spectrometry (GC–MS, Agilent 6890–5973). A total of 5 mg soot was first ultrasonically extracted for 10 min using 10 mL of dichloromethane (CH_2Cl_2), which was filtered through a quartz sand filter. The obtained supernatant liquid was subsequently concentrated using the N_2 blowing method for final analysis. The gas chromatograph was equipped with a DB-5MS 30 m × 0.25 mm × 0.25 mm capillary column and the mass spectrometer employed a quadrupole mass filter with a 70 eV electron impact ionizer. The temperature of the programmed temperature vaporizer was held at 270 °C. The initial oven temperature was set to 40 °C for 2 min and then increased step by step to 150 °C (by 5 °C min^{-1}) for 5 min, 280 °C (by 10 °C min^{-1}) for 10 min and 320 °C (by 10 °C min^{-1}) for 5 min.

For ion chromatography (IC) measurement, about 5 mg of soot particles were extracted by ultrasonication with 10 mL ultrapure water (18.2 MΩ cm) for 10 min. Then, the extract was filtered through a 0.22 mm PTFE membrane filter. The obtained solution was analyzed using a Wayee IC-6200 ion chromatography system equipped with an SI-524E anionic analytical column. An eluent of 10 mM KOH was used at a flow rate of 1.0 mL min^{-1}.

2.3 Hygroscopic properties of soot

The hygroscopic properties of soots were investigated using a vapor sorption analyzer (VSA, Q5000 SA, TA Instruments), which has been applied to study hygroscopicity of atmospherically relevant particles in previous work (Chen et al., 2019; Gu et al., 2017). VSA utilizes a highly sensitive balance to measure the mass change in a sample as a function of RH at a given temperature. The instrument has a measurement range of 0–100 mg with a sensitivity of 0.01 µg, allowing for precise analysis. The temperature could be controlled in the range of 5–85 °C with an accuracy of 0.1 °C, and RH could be regulated in the range of 0 %–98 % with an absolute accuracy of 1 %. To ensure the accuracy of RH measurements, we routinely measured deliquescence relative humidities (DRHs) of NaCl, $(NH_4)_2SO_4$ and KCl, and the difference between measured and theoretical DRHs did not exceed 1 %, confirming the reliability and accuracy of the instrument.

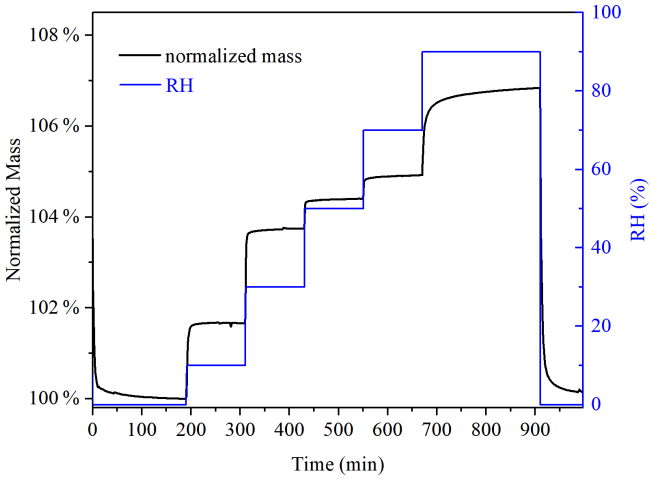

Figure 1. RH (blue curve, right *y* axis) and normalized sample mass (black curve, left *y* axis) as a function of experimental time during one experiment in which hygroscopic properties of U-soot were examined at 25 °C.

Hygroscopicity of soot was investigated at 25 °C. Figure 1 displays the change in RH and normalized sample mass with experimental time in a typical experiment. U-soot was dried at <1 % RH, and the sample mass under dry conditions was typically 1–5 mg. After that, RH increased step by step from 10 %–90 %, with an increase of 20 % per step. At each point, the adsorption of water on samples was considered to reach an equilibrium when its mass change was <0.05 % within 60 min.

3 Result and discussion

3.1 The morphology and vapor adsorption isotherms of various types of soot

Figure 2 shows TEM images of soot samples. All soot samples exhibit a long chain-like aggregate shape composed of typical spherical particles, which is consistent with previous studies (Han et al., 2012; Liu et al., 2010).

Figure 3 shows the diameter distribution of soot particles. Particles exhibit a relatively uniform particle size distribution. Notably, the proportion of spherical particles with a large diameter (>35 nm) of aged U-soot was slightly greater than that of fresh U-soot. Nevertheless, the average particle diameters ($\overline{d}_p$) of U-soot and SO_2 aged U-soot are 39.55 and 41.60 nm, respectively, suggesting a weak effect of SO_2 het-

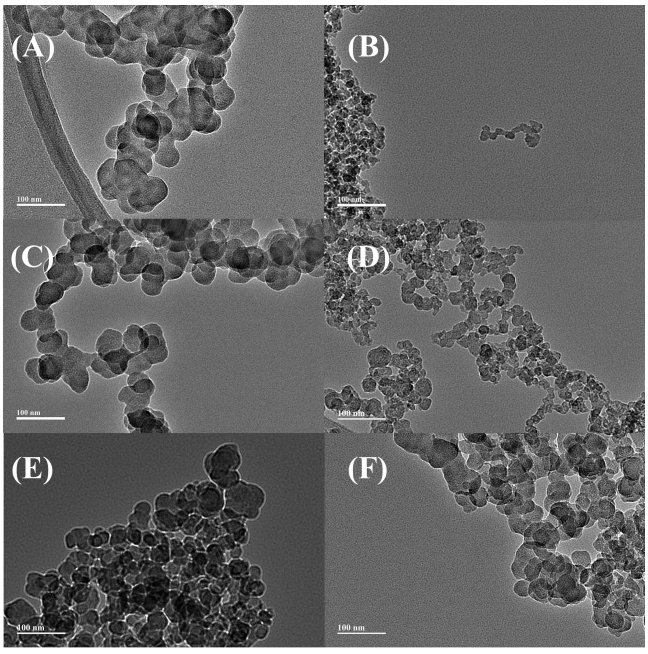

Figure 2. TEM images of *n*-hexane flame soot **(a)**, decane flame soot **(b)**, toluene flame soot **(c)**, diesel soot **(d)** and U-soot aggregates **(e)** before and **(f)** after aging with 5 ppm of SO_2 for 10 h.

erogeneous reaction on the size distribution of U-soot particles.

Figure 4 shows the normalized sample mass (normalized to that at <1 % RH, m/m_0) as a function of RH for five types of soot. Three types of prepared soots (*n*-hexane flame soot, decane flame soot and toluene flame soot) exhibited lower water adsorption per unit mass sample under each RH condition compared to DS and U-soot particles. Specifically, at 90 % RH, DS showed the highest water adsorption among all soot samples, with a m/m_0 value of 1.138, followed by U-soot with a value of 1.067. Moreover, among the three prepared soots, decane flame soot exhibited the highest hygroscopicity with a normalized sample mass of 1.054 at 90 % RH.

In order to further analyze the adsorption characteristics of water on soot, the isotherms of soot were fitted with the Brunauer–Emmett–Teller (BET) equation. As shown in Fig. 4, the isotherms of prepared soot and U-soot could be well fitted with a three-parameter BET equation with the assumption of limited adsorbed water layers as following Eq. (1) (Brunauer et al., 1938; Goodman et al., 2001; Ma et al., 2010; Tang et al., 2016):

$$V = \frac{V_m c \frac{P}{P_0}}{1-\frac{P}{P_0}} \times \frac{1-(n+1)\left(\frac{P}{P_0}\right)^n + n\left(\frac{P}{P_0}\right)^{n+1}}{1+(c-1)\frac{P}{P_0} - c\left(\frac{P}{P_0}\right)^{n+1}}, \quad (1)$$

where V is the volume of gas adsorbed at equilibrium pressure P, V_m is the volume of gas necessary to cover the surface of the adsorbent with a complete monolayer and P_0 is the saturation vapor pressure of the adsorbing gas at that temperature. n is an adjustable parameter given as the maximum number of layers of the adsorbing gas and is related to the pore size and properties of adsorbent. As a result, multilayer formation of adsorbing gas is limited to n layers at large values of P/P_0. The parameter c is the temperature-dependent constant related to the enthalpies of adsorption of the first and higher layers through Eq. (2) (Brunauer et al., 1938):

$$c = \exp\left(\frac{\Delta H_2^0 - \Delta H_1^0}{RT}\right), \quad (2)$$

where ΔH_1^0 is the standard enthalpy of adsorption of the first layer, and ΔH_2^0 is the standard enthalpy of adsorption on subsequent layers and is taken as the standard enthalpy of condensation, R is the gas constant, and T is the temperature in kelvin.

For DS, a notable increase in sample mass was observed between 70 % and 90 % RH. This can be attributed to a significant rise in the number of adsorbed water layers within this specific RH range, which leads to the inability to describe the adsorption isotherm using the three-parameter BET equation. However, the two-parameter BET equation (Eq. 3), assuming an unlimited number of adsorbed water layers, provides a better fit for the observed adsorption behavior of DS particles (Brunauer et al., 1938):

$$V = \frac{V_m c P}{(P_0 - P)\{1+(c-1)(P/P_0)\}}. \quad (3)$$

The fitted parameters, as shown in Table 1, provide valuable insights into the water adsorption behavior of different types of soot. The threshold relative humidity for one monolayer (MRH) for the fresh prepared soots is approximately 70 % RH. However, both U-soot and DS exhibit significantly lower MRH values ($MRH_{DS} = 15$ % RH, $MRH_{U\text{-}soot} = 25.5$ % RH) compared to fresh prepared soot. This suggests that U-soot and DS have a higher affinity for water uptake at lower RH levels than fresh soot. At 90 % RH, prepared soot and U-soot particles were found to have approximately 1.2 and 2.1 layers of surface water adsorbed, respectively. Interestingly, DS showed around 9.5 layers adsorbed at 90 % RH, indicating a strong propensity for water adsorption.

The water-soluble ions like SO_4^{2-} and NO_3^- in soot samples were analyzed by IC, and the corresponding results are presented in Table 2. It was observed that the content of NO_3^- in all soot samples, except for DS, was approximately 0.2 µg mg^{-1}. However, DS exhibited a higher NO_3^- content of 1.44 µg mg^{-1}, which could be due to the aging of high-concentration NO_x coexisting in the exhaust pipe. Regarding SO_4^{2-}, the fresh prepared soots did not show any detectable levels of SO_4^{2-}. In contrast, both U-soot and DS displayed notable amounts of SO_4^{2-}, with U-soot having a content of 2.54 µg mg^{-1} and DS having the highest content of

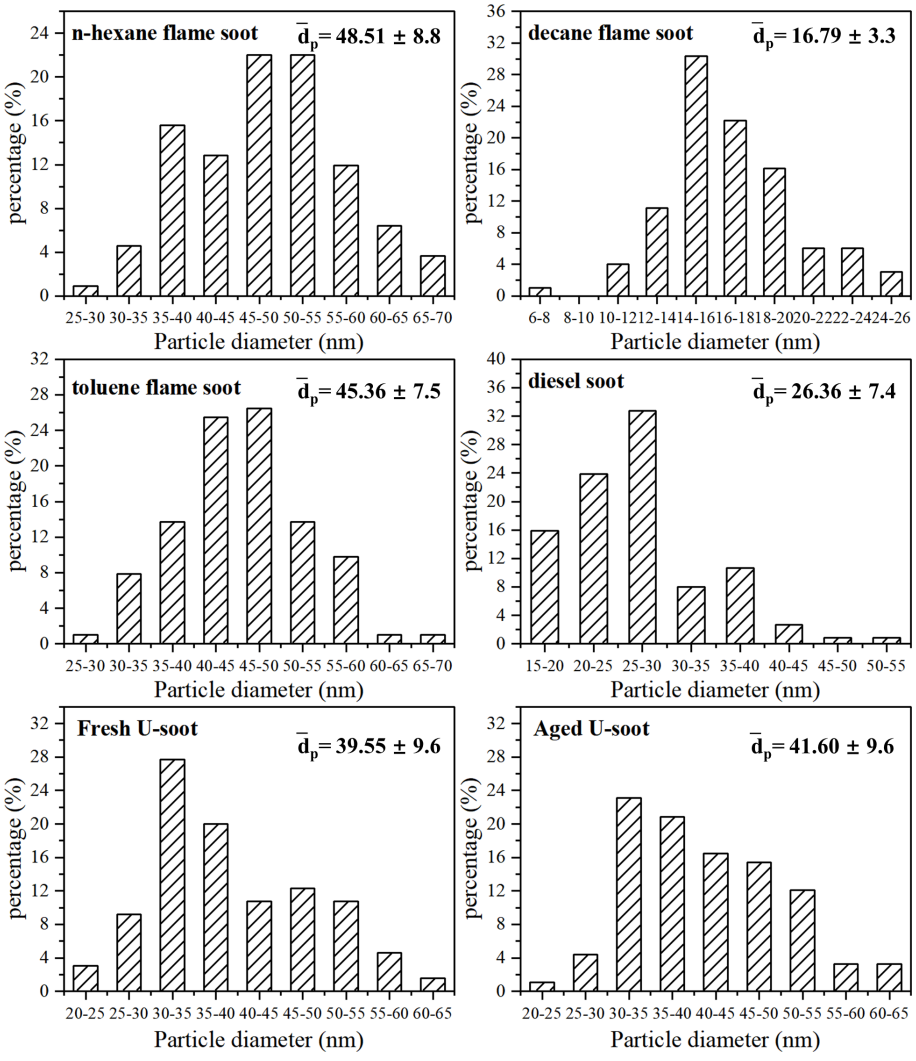

Figure 3. Diameter distribution of *n*-hexane flame soot, decane flame soot, toluene flame soot and diesel soot and U-soot particles before and after aging with 5 ppm of SO_2 for 10 h.

11.46 µg mg^{-1}. These results indicate that water-soluble inorganic ions (e.g., nitrates and sulfates) are a dominant factor for enhancing the hygroscopicity of soot, which is consistent with previous studies (Carrico et al., 2010; Popovicheva et al., 2010).

3.2 The factors controlling the hygroscopic properties of prepared soot

Compared with DS and U-soot, prepared soots are more hydrophobic (Fig. 4) due to containing fewer water-soluble inorganic ions (Table 2). However, there are still significant differences in the hygroscopic behavior of soots prepared from different fuels. In order to analyze the differences in the hygroscopicity of different prepared soot, the relative content and species of OC and the microstructure of soot were characterized. It was found that the *n*-hexane flame soot has the highest OC/EC ratio, followed by toluene flame soot, and decane flame soot has the lowest OC/EC ratio (Table 2). It should be noted that the ratio of OC/EC is negatively correlated with their hygroscopicity, indicating that organic carbon is not conducive to the adsorption of water on the surface of soot. The impact of OC on the hygroscopicity of soot is still a subject of debate. Some field observation results have indicated that particles with a high OC/EC ratio were preferentially removed by precipitation and that the condensation of photochemically generated secondary organic carbon on soot particles could cause enhancement of hygroscopicity (Dasch and Cadle, 1989; Li et al., 2018). However, H-TDMA measurements have shown that neither hygroscopicity nor droplet activation of the fresh propane soot particles depends on the OC content (Henning et al., 2012). Therefore, it is necessary to analyze the specific OC species present in

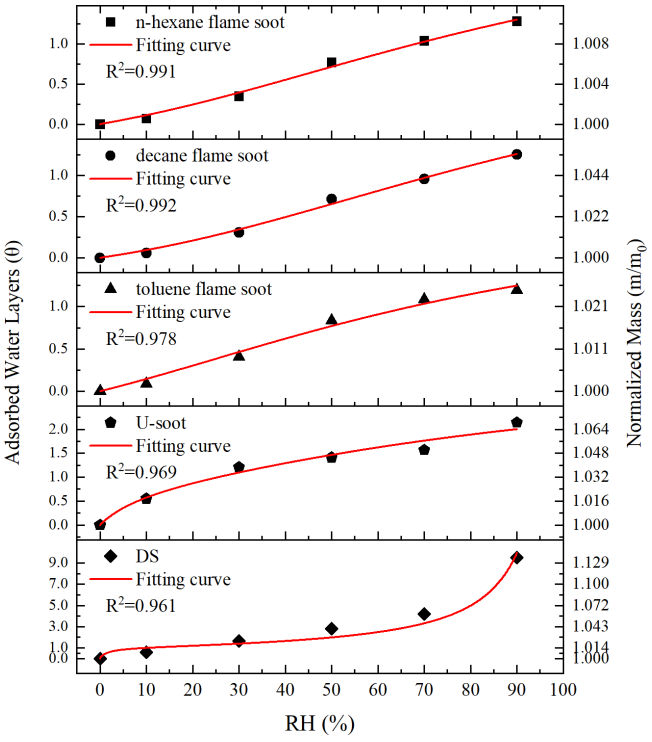

Figure 4. Water adsorption isotherms of soots, fitting curves (lines) with BET equation and the measured sample mass change (normalized to that at <1 % RH, i.e., m/m_0) of soots as a function of RH (up to 90 % RH).

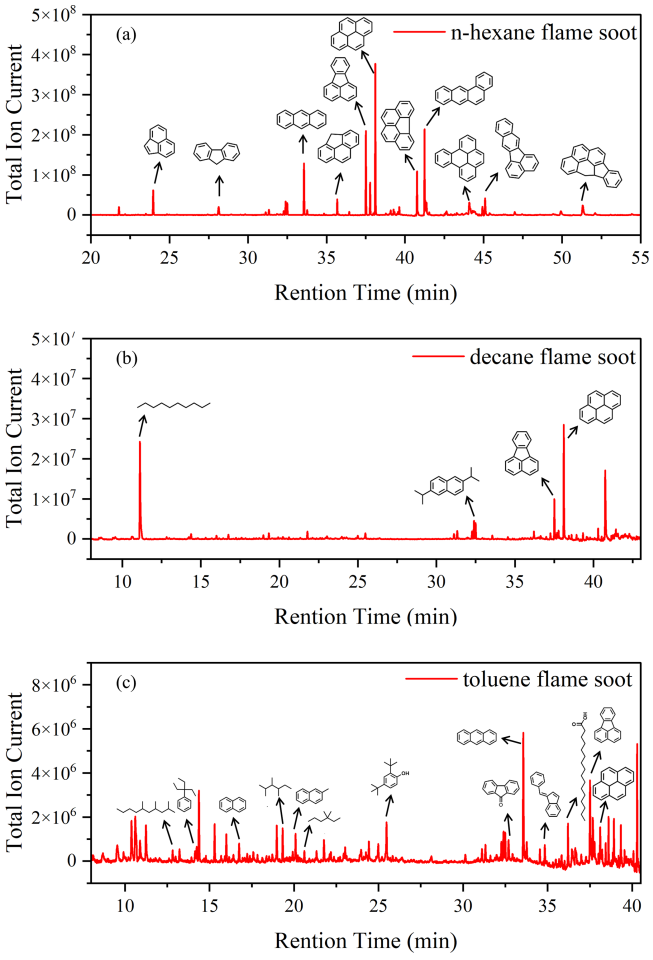

Figure 5. Total ion chromatogram extracts of prepared soots. **(a)** *n*-Hexane flame soot. **(b)** Decane flame soot. **(c)** Toluene flame soot.

prepared soot particles to gain a better understanding of their role in hygroscopicity.

In order to obtain the composition of OC in different types of soot, the samples were extracted by CH_2Cl_2, and the extract was analyzed by GC-MS. Figure 5 shows the GC-MS analysis of OC extracted from different prepared soot. The major components are polyaromatic hydrocarbons (PAHs) like anthracene, fluoranthene and pyrene in all soot samples. It is well known that PAHs are usually formed simultaneously with soot during combustion. In *n*-hexane flame soot, PAHs are the main OC, while other components are scarce, which is consistent with the results of Han et al. (2012). For decane and toluene flame soot, long-chain alkanes such as decane or 2,3,4-trimethyl-hexane are present in the OC fraction. The characteristic features and peculiarities of the adsorption of water vapor on soot are primarily caused by the tendency of polar water molecules to form hydrogen bonds (Vartapetyan and Voloshchuk, 1995). However, PAHs are weakly polar organic compounds. Thus, the ability of π electrons in the PAH aromatic ring to form weak hydrogen bonds with water molecules or the interactions with water molecules are either almost absent or are negligible (Lobunez, 1960). The oxygen-containing functional groups of organic compounds are substantial centers for the formation of hydrogen bonds with water molecules. In toluene flame soot, certain OC compounds (2,4-Di-tert-butylphenol, palmitic acid and 9-fluorenone) possess oxygen-containing functional groups like hydroxyl groups, carboxyl groups and quinone. However, these OC compounds also contain substantial hydrophobic parts (aromatic ring and hydrocarbon part). Despite a small amount, the contribution of these hydrophobic functional groups to the hygroscopicity could be dominant (Kireeva et al., 2010). For long-chain alkanes found in decane and toluene flame soot, they are typically considered hydrophobic. In general, OC constituents detected in these prepared soot samples could impede water adsorption on soot surfaces. Hence, the presence of these OC compounds leads to hydrophobic characteristics and diminishes the water adsorption capacity of prepared soot.

In order to study the relationship between the microstructure and vapor adsorption capacity of soot, Raman analysis on soot samples was conducted. Figure 6 shows the first-order Raman spectra of three prepared soots with good curve-fitting results (R^2>0.982), which display well-known bands of soot near 1580 (G band) and 1360 cm^{-1} (D band).

Table 1. Adsorption parameters for water uptake on soot.

Soot	BET area ($m^2\ g^{-1}$)	MRH (%)	n	c	R^2
n-Hexane flame soot	26.27	68.0	2.84	1.01	0.991
Toluene flame soot	70.97	67.2	2.47	1.37	0.978
Decane flame soot	147.36	72.0	2.92	0.83	0.992
DS	47.93	15.0	–	66.95	0.961
U-soot	97.24	25.5	3.34	9.57	0.969
U-soot aged 2 h	99.80	24.4	3.42	10.67	0.973
U-soot aged 6 h	101.46	25.0	3.59	9.82	0.956
U-soot aged 10 h	98.96	26.2	3.82	8.58	0.944

Table 2. Mass concentration of SO_4^{2-} and NO_3^- and the ratio of OC/EC of soots.

Soot	Mass concentration of SO_4^{2-} ($\mu g\ mg^{-1}$)	Mass concentration of NO_3^- ($\mu g\ mg^{-1}$)	OC/EC
n-Hexane flame soot	0.00	0.19	0.41 ± 0.02
Toluene flame soot	0.00	0.18	0.24 ± 0.04
Decane flame soot	0.00	0.22	0.16 ± 0.06
DS	11.46	1.44	0.14 ± 0.02
U-soot	2.55	0.24	0.12 ± 0.03
U-soot aged 2 h	4.83	0.20	–
U-soot aged 6 h	7.14	0.19	–
U-soot aged 10 h	9.61	0.20	–

The G band is a typical characteristic of crystalline graphite, while the D band is only observed for disordered graphite. A detailed analysis of the first-order Raman spectra was performed using the five-band fitting procedure proposed by Sadezky (Sadezky et al., 2005). Four Lorentzian-shaped bands (D1, D2, D4 and G, centered at about 1360, 1620, 1180 and 1580 cm^{-1}, respectively) and one Gaussian-shaped band (D3, centered at around 1500 cm^{-1}) were used in the curve-fitting process (Sadezky et al., 2005; Ivleva et al., 2007; Liu et al., 2010). The D1 band arises from the A_{1g} symmetry mode of the disordered graphitic lattice located at the graphene layer edges. The D2 band is attributed to the E_{2g} symmetry stretching mode of the disordered graphitic lattice located at surface graphene layers. The D3 band originates from the amorphous carbon fraction of soot. The D4 band is related to the A_{1g} symmetry mode of the disordered graphitic lattice or C–C and C = C stretching vibrations of polyene-like structures; polyenes and ionic impurities also contribute to the D4 band (Sze et al., 2001; Sadezky et al., 2005). The G band is assigned to the ideal graphitic lattice with E_{2g} symmetry vibration mode. The integral intensity ratio (I_D/I_G) of D and G bands was found to be related to the graphite crystallite size L_a (as determined by X-ray) (Knight and White, 1989; Schwan et al., 1996):

$$\frac{44}{L_a} = \left(\frac{I_D}{I_G}\right). \quad (4)$$

The intensities of the D and G bands have been widely determined using the sum of the D1 and D4 bands and the sum of the D2 and G bands (Knauer et al., 2009). Table 3 shows similar changing trends between the I_{D4}/I_G of the three prepared soot samples and their hygroscopicity, while the L_a of the three prepared soot samples exhibits a negative correlation. These results imply that disordered graphitic lattice, polyenes or ionic impurities (D4) could potentially serve as adsorption sites for water molecules. Moreover, graphite crystallite with a smaller size could have a higher adsorption capacity of water in soot.

3.3 The effect of aging process on the hygroscopicity of soot

Based on the hygroscopicity measurements of U-soot and DS (Fig. 4 and Table 2), it is evident that the coating water-soluble inorganic ions (e.g., sulfates and nitrates) can enhance the hygroscopicity of soot particles. Field observations have shown that the mass fractions of ammonium, sulfate and nitrate increase with the aging of fresh biomass burning particles (Pratt et al., 2011). To investigate the impact of sulfate formation during the aging process on soot hygroscopicity, we aged U-soot with SO_2 for different durations and measured their hygroscopic properties accordingly. The results revealed an increase in sulfate ions on U-soot with longer aging times (Table 2), while the MRH of U-soot remains relatively unchanged with SO_2 aging (Table 1). However, at

Table 3. Parameters I_{D1}/I_G, I_{D4}/I_G, I_D/I_G and L_a of n-hexane, decane and toluene flame soot.

Fuels	I_{D1}/I_G	I_{D4}/I_G	I_D/I_G	L_a (Å)
n-Hexane	2.59 ± 0.13	0.33 ± 0.01	2.87 ± 0.13	15.34 ± 0.69
Toluene	2.87 ± 0.03	0.42 ± 0.09	3.23 ± 0.09	13.62 ± 0.38
Decane	2.69 ± 0.08	0.75 ± 0.01	3.49 ± 0.15	12.63 ± 0.53

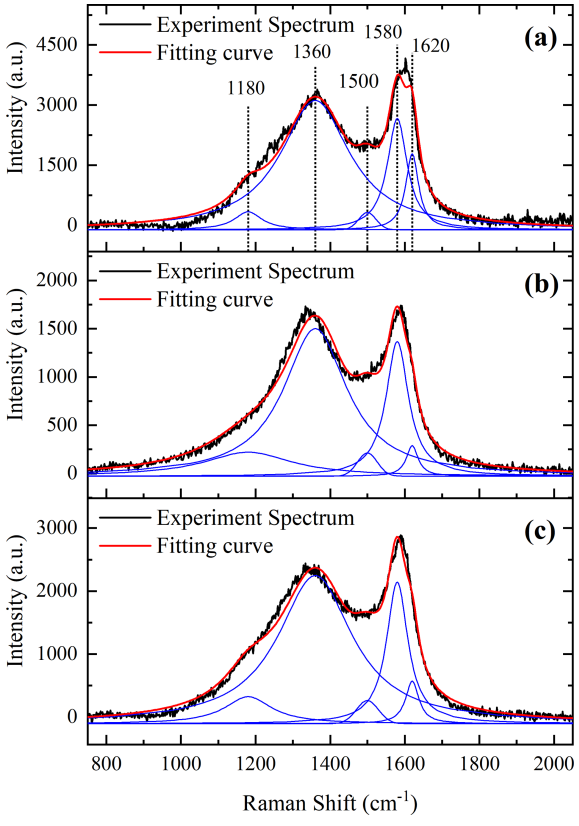

Figure 6. Raman spectra of **(a)** n-hexane, **(b)** decane and **(c)** toluene flame soot.

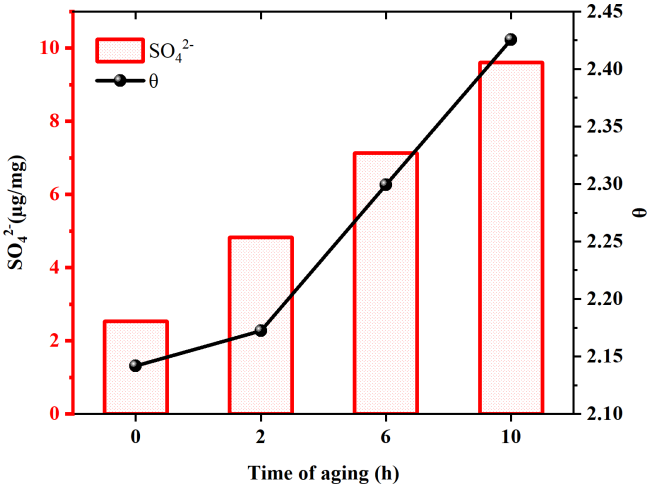

Figure 7. Amounts of sulfates on U-soot and the adsorbed water layers (θ) at 90 % RH of U-soot as a function of the time of aging.

90 % RH, the adsorbed water layers on U-soot increase with increasing aging times (Fig. 7). It should be noted that there is a good linear relationship ($R^2 = 0.9997$) between sulfate formed from SO_2 aging and adsorbed water mass at 90 % RH, where a corresponding water absorption mass increased by 1.82 µg for every 1 µg of SO_4^{2-} produced on the surface of U-soot.

Our previous study found that the heterogeneous reaction between SO_2 and soot leads to the formation of sulfuric acid coating on soot (Zhang et al., 2022b). In this study, the sulfate detected on U-soot could also exist in the form of sulfuric acid. However, IC results demonstrated that the amount of newly generated sulfate on U-soot after 10 h of aging was only 0.706 % of its original mass (Table 2). This small amount is insufficient to cause a significant difference in mass growth at low relative humidity and causes little change in MRH. However, Kireeva et al. (2010) showed that the water adsorption isotherm of graphitized thermal soot coated with a small quantity of sulfuric acid showed a significant increase in the mass growth factor at relative humidity levels above 90 % (Kireeva et al., 2010). Zhang et al. (2008) found that coating with sulfuric acid could increase the mass growth factor of soot to above 1.2 at 80 % RH relative to fresh particles (Zhang et al., 2008). Our results also demonstrated that a noticeable augmentation in the amount of water adsorbed on SO_2 aged soot at 90 % RH, which is positively correlated with the amount of sulfate generated. Based on these findings, it can be concluded that varying amounts of sulfuric acid produced through heterogeneous oxidation on the surface of soot lead to noticeable differences in the amount of adsorbed water at high relative humidity. These findings are consistent with previous studies that coating with sulfuric acid can increase the hygroscopicity and ice nucleation activation of soot (Demott et al., 1999; Möhler et al., 2005; Wyslouzil et al., 1994).

4 Conclusions

In this study, we employed a vapor sorption analyzer to investigate the hygroscopicity of soot particles from different sources and at different stages of aging with sulfur dioxide. Multiple characterizations of soot particles were also per-

formed. DS and U-soot contained water-soluble ions, such as sulfates and nitrates, which enabled them to undergo monolayer adsorption at lower relative humidity and increase the number of water absorption layers at higher relative humidity. In contrast, fresh prepared soot particles, which have negligible amounts of water-soluble ions, were more hydrophobic. Their hygroscopicity mainly depended on the organic carbon content and microstructure. A lower content of hydrophobic OC and more disordered graphitic lattice, polyenes or ionic impurities made prepared soot particles more prone to water adsorption. The aging of U-soot particles with SO_2 resulted in the formation of water-soluble sulfate ions, which promotes an increase in the hygroscopicity of soot particles. This study analyzed the key factors determining the hygroscopic property of soot, which can improve our understanding of the hygroscopic behavior of fresh soot and help to evaluate changes in hygroscopicity during the heterogeneous reactions of soot particles with pollutant gases in future studies.

Data availability. The experimental data are available upon request to the first or corresponding authors.

Author contributions. QM contributed to the conception of the study, ZS and LC designed and conducted this experiment, and YL helped to prepare samples. QM, PZ, TC, BC, MT and HH helped perform the analysis with constructive discussions. ZS and QM wrote the paper with input from all coauthors. All authors contributed to the final paper.

Competing interests. The contact author has declared that none of the authors has any competing interests.

Disclaimer. Publisher's note: Copernicus Publications remains neutral with regard to jurisdictional claims made in the text, published maps, institutional affiliations, or any other geographical representation in this paper. While Copernicus Publications makes every effort to include appropriate place names, the final responsibility lies with the authors.

Acknowledgements. The authors warmly thank the technical support provided by the State Key Joint Laboratory of Environment Simulation and Pollution Control, Research Center for Eco-Environmental Sciences, Chinese Academy of Sciences and the State Key Laboratory of Organic Geochemistry, Guangzhou Institute of Geochemistry, Chinese Academy of Sciences for measurement in this work. Moreover, the authors wish to thank the anonymous reviewers for their valuable comments and suggestions that allowed us to greatly improve the paper.

Financial support. This research has been supported by the National Key R&D Program of China (grant no. 2022YFC3701004), the National Natural Science Foundation of China (grant no. 22188102), and the Youth Innovation Promotion Association, CAS (grant no. Y2022021).

Review statement. This paper was edited by Zhibin Wang and reviewed by three anonymous referees.

References

Bond, T. C., Doherty, S. J., Fahey, D. W., Forster, P. M., Berntsen, T., DeAngelo, B. J., Flanner, M. G., Ghan, S., Kaercher, B., Koch, D., Kinne, S., Kondo, Y., Quinn, P. K., Sarofim, M. C., Schultz, M. G., Schulz, M., Venkataraman, C., Zhang, H., Zhang, S., Bellouin, N., Guttikunda, S. K., Hopke, P. K., Jacobson, M. Z., Kaiser, J. W., Klimont, Z., Lohmann, U., Schwarz, J. P., Shindell, D., Storelvmo, T., Warren, S. G., and Zender, C. S.: Bounding the role of black carbon in the climate system: A scientific assessment, J. Geophys. Res.-Atmos., 118, 5380–5552, https://doi.org/10.1002/jgrd.50171, 2013.

Brunauer, S., Emmett, P. H., and Teller, E.: Adsorption of gases in multimolecular layers, J. Am. Chem. Soc., 60, 309–319, https://doi.org/10.1021/ja01269a023, 1938.

Cappa, C. D., Onasch, T. B., Massoli, P., Worsnop, D. R., Bates, T. S., Cross, E. S., Davidovits, P., Hakala, J., Hayden, K. L., Jobson, B. T., Kolesar, K. R., Lack, D. A., Lerner, B. M., Li, S.-M., Mellon, D., Nuaaman, I., Olfert, J. S., Petaja, T., Quinn, P. K., Song, C., Subramanian, R., Williams, E. J., and Zaveri, R. A.: Radiative Absorption Enhancements Due to the Mixing State of Atmospheric Black Carbon, Science, 337, 1078–1081, https://doi.org/10.1126/science.1223447, 2012.

Carrico, C. M., Petters, M. D., Kreidenweis, S. M., Sullivan, A. P., McMeeking, G. R., Levin, E. J. T., Engling, G., Malm, W. C., and Collett Jr., J. L.: Water uptake and chemical composition of fresh aerosols generated in open burning of biomass, Atmos. Chem. Phys., 10, 5165–5178, https://doi.org/10.5194/acp-10-5165-2010, 2010.

Chen, L., Chen, Y., Chen, L., Gu, W., Peng, C., Luo, S., Song, W., Wang, Z., and Tang, M.: Hygroscopic Properties of 11 Pollen Species in China, ACS Earth Space Chem., 3, 2678–2683, https://doi.org/10.1021/acsearthspacechem.9b00268, 2019.

Chow, J. C., Watson, J. G., Pritchett, L. C., Pierson, W. R., Frazier, C. A., and Purcell, R. G.: The Dri Thermal Optical Reflectance Carbon Analysis System – Description, Evaluation And Applications in United-States Air-Quality Studies, Atmos. Environ. Pt. A, 27, 1185–1201, https://doi.org/10.1016/0960-1686(93)90245-t, 1993.

Dasch, J. M. and Cadle, S. H.: Atmospheric Carbon Particles in the Detroit Urban Area: Wintertime Sources and Sinks, Aerosol Sci. Technol., 10, 236–248, https://doi.org/10.1080/02786828908600508, 1989.

DeMott, P. J., Chen, Y., Kreidenweis, S. M., Rogers, D. C., and Sherman, D. E.: Ice formation by black carbon particles, Geophys. Res. Lett., 26, 2429–2432, https://doi.org/10.1029/1999gl900580, 1999.

Forster, P., Ramaswamy, V., Artaxo, P., Berntsen, T., Betts, R., Fahey, D. W., Haywood, J., Lean, J., Lowe, D. C., Myhre, G., Nganga, J., Prinn, R., Raga, G., Schulz, M., and Van Dorland, R.: Changes in Atmospheric Constituents and in Radiative Forcing, Ar4 Climate Change 2007: The Physical Science Basis: Contribution of Working Group I to the Fourth Assessment Report of the Intergovernmental Panel on Climate Change, edited by: Solomon, S., Qin, D., Manning, M., Chen, Z., Marquis, M., Averyt, K. B., Tignor, M., and Miller, H. L., Cambridge University Press, Cambridge, United Kingdom and New York, NY, 129–243, ISBN: 9780521880091, 2007.

Friedman, B., Kulkarni, G., Beranek, J., Zelenyuk, A., Thornton, J. A., and Cziczo, D. J.: Ice nucleation and droplet formation by bare and coated soot particles, J. Geophys. Res.-Atmos., 116, D17203, https://doi.org/10.1029/2011jd015999, 2011.

Goodman, A. L., Bernard, E. T., and Grassian, V. H.: Spectroscopic study of nitric acid and water adsorption on oxide particles: Enhanced nitric acid uptake kinetics in the presence of adsorbed water, J. Phys. Chem. A, 105, 6443–6457, https://doi.org/10.1021/jp003722l, 2001.

Gu, W., Li, Y., Zhu, J., Jia, X., Lin, Q., Zhang, G., Ding, X., Song, W., Bi, X., Wang, X., and Tang, M.: Investigation of water adsorption and hygroscopicity of atmospherically relevant particles using a commercial vapor sorption analyzer, Atmos. Meas. Tech., 10, 3821–3832, https://doi.org/10.5194/amt-10-3821-2017, 2017.

Han, C., Liu, Y., and He, H.: Heterogeneous reaction of NO_2 with soot at different relative humidity, Environ. Sci. Pollut. Res. Int., 24, 21248–21255, https://doi.org/10.1007/s11356-017-9766-y, 2017.

Han, C., Liu, Y., Liu, C., Ma, J., and He, H.: Influence of combustion conditions on hydrophilic properties and microstructure of flame soot, J. Phys. Chem. A, 116, 4129–4136, https://doi.org/10.1021/jp301041w, 2012.

He, G., Ma, J., Chu, B., Hu, R., Li, H., Gao, M., Liu, Y., Wang, Y., Ma, Q., Xie, P., Zhang, G., Zeng, X. C., Francisco, J. S., and He, H.: Generation and Release of OH Radicals from the Reaction of H_2 O with O_2 over Soot, Angew. Chem. Int. Ed. Engl., 61, e202201638, https://doi.org/10.1002/anie.202201638, 2022.

He, G. Z. and He, H.: Water Promotes the Oxidation of SO_2 by O-2 over Carbonaceous Aerosols, Environ. Sci. Technol., 54, 7070–7077, https://doi.org/10.1021/acs.est.0c00021, 2020.

Henning, S., Ziese, M., Kiselev, A., Saathoff, H., Moehler, O., Mentel, T. F., Buchholz, A., Spindler, C., Michaud, V., Monier, M., Sellegri, K., and Stratmann, F.: Hygroscopic growth and droplet activation of soot particles: uncoated, succinic or sulfuric acid coated, Atmos. Chem. Phys., 12, 4525–4537, https://doi.org/10.5194/acp-12-4525-2012, 2012.

Henning, S., Wex, H., Hennig, T., Kiselev, A., Snider, J. R., Rose, D., Dusek, U., Frank, G. P., Pöschl, U., Kristensson, A., Bilde, M., Tillmann, R., Kiendler-Scharr, A., Mentel, T. F., Walter, S., Schneider, J., Wennrich, C., and Stratmann, F.: Soluble mass, hygroscopic growth, and droplet activation of coated soot particles during LACIS Experiment in November (LExNo), J. Geophys. Res.-Atmos., 115, D11206, https://doi.org/10.1029/2009jd012626, 2010.

Hu, D., Wang, Y., Yu, C., Xie, Q., Yue, S., Shang, D., Fang, X., Joshi, R., Liu, D., Allan, J., Wu, Z., Hu, M., Fu, P., and McFiggans, G.: Vertical profile of particle hygroscopicity and CCN effectiveness during winter in Beijing: insight into the hygroscopicity transition threshold of black carbon, Faraday Discuss., 226, 239–254, https://doi.org/10.1039/d0fd00077a, 2021.

Ivleva, N. P., Messerer, A., Yang, X., Niessner, R., and Poeschl, U.: Raman microspectroscopic analysis of changes in the chemical structure and reactivity of soot in a diesel exhaust aftertreatment model system, Environ. Sci. Technol., 41, 3702–3707, https://doi.org/10.1021/es0612448, 2007.

Janssen, N. A. H., Hoek, G., Simic-Lawson, M., Fischer, P., van Bree, L., ten Brink, H., Keuken, M., Atkinson, R. W., Anderson, H. R., Brunekreef, B., and Cassee, F. R.: Black Carbon as an Additional Indicator of the Adverse Health Effects of Airborne Particles Compared with PM_{10} and $PM_{2.5}$, Environ. Health Persp., 119, 1691–1699, https://doi.org/10.1289/ehp.1003369, 2011.

Kireeva, E. D., Popovicheva, O. B., Khokhlova, T. D., and Shoniya, N. K.: Laboratory simulation of the interaction of water molecules with carbonaceous aerosols in the atmosphere, Mosc. U. Phys. Bull., 65, 510–515, https://doi.org/10.3103/s0027134910060159, 2010.

Knauer, M., Schuster, M. E., Su, D. S., Schlögl, R., Niessner, R., and Ivleva, N. P.: Soot Structure and Reactivity Analysis by Raman Microspectroscopy, Temperature-Programmed Oxidation, and High-Resolution Transmission Electron Microscopy, J. Phys. Chem. A, 113, 13871–13880, https://doi.org/10.1021/jp905639d, 2009.

Knight, D. S. and White, W. B.: Characterization of diamond films by Raman spectroscopy, J. Mater. Res., 4, 385–393, https://doi.org/10.1557/JMR.1989.0385, 1989.

Li, C., Hu, Y., Chen, J., Ma, Z., Ye, X., Yang, X., Wang, L., Wang, X., and Mellouki, A.: Physiochemical properties of carbonaceous aerosol from agricultural residue burning: Density, volatility, and hygroscopicity, Atmos. Environ., 140, 94–105, https://doi.org/10.1016/j.atmosenv.2016.05.052, 2016.

Li, K., Ye, X., Pang, H., Lu, X., Chen, H., Wang, X., Yang, X., Chen, J., and Chen, Y.: Temporal variations in the hygroscopicity and mixing state of black carbon aerosols in a polluted megacity area, Atmos. Chem. Phys., 18, 15201–15218, https://doi.org/10.5194/acp-18-15201-2018, 2018.

Liao, H., Chang, W., and Yang, Y.: Climatic Effects of Air Pollutants over China: A Review, Adv. Atmos. Sci., 32, 115–139, https://doi.org/10.1007/s00376-014-0013-x, 2015.

Lin, W., Huang, W., Zhu, T., Hu, M., Brunekreef, B., Zhang, Y., Liu, X., Cheng, H., Gehring, U., Li, C., and Tang, X.: Acute Respiratory Inflammation in Children and Black Carbon in Ambient Air before and during the 2008 Beijing Olympics, Environ. Health Persp., 119, 1507–1512, https://doi.org/10.1289/ehp.1103461, 2011.

Liu, D., Whitehead, J., Alfarra, M. R., Reyes-Villegas, E., Spracklen, D. V., Reddington, C. L., Kong, S., Williams, P. I., Ting, Y.-C., Haslett, S., Taylor, J. W., Flynn, M. J., Morgan, W. T., McFiggans, G., Coe, H., and Allan, J. D.: Black-carbon absorption enhancement in the atmosphere determined by particle mixing state, Nat. Geosci., 10, 184–188, https://doi.org/10.1038/ngeo2901, 2017.

Liu, Y., He, G., Chu, B., Ma, Q., and He, H.: Atmospheric heterogeneous reactions on soot: A review, Fundament. Res., 3, 579–591, https://doi.org/10.1016/j.fmre.2022.02.012, 2023.

Liu, Y., Liu, C., Ma, J., Ma, Q., and He, H.: Structural and hygroscopic changes of soot during heterogeneous reac-

tion with O_3, Phys. Chem. Chem. Phys., 12, 10896–10903, https://doi.org/10.1039/c0cp00402b, 2010.

Lobunez, W.: Book Reviews: The Hydrogen Bond., Text. Res. J., 30, 1006–1007, https://doi.org/10.1177/004051756003001217, 1960.

Ma, Q., He, H., and Liu, Y.: In situ DRIFTS study of hygroscopic behavior of mineral aerosol, J. Environ. Sci., 22, 555–560, https://doi.org/10.1016/s1001-0742(09)60145-5, 2010.

Matsui, H., Koike, M., Kondo, Y., Moteki, N., Fast, J. D., and Zaveri, R. A.: Development and validation of a black carbon mixing state resolved three-dimensional model: Aging processes and radiative impact, J. Geophys. Res.-Atmos., 118, 2304–2326, https://doi.org/10.1029/2012jd018446, 2013.

Möhler, O., Büttner, S., Linke, C., Schnaiter, M., Saathoff, H., Stetzer, O., Wagner, R., Krämer, M., Mangold, A., Ebert, V., and Schurath, U.: Effect of sulfuric acid coating on heterogeneous ice nucleation by soot aerosol particles, J. Geophys. Res., 110, D11210, https://doi.org/10.1029/2004jd005169, 2005.

Ohata, S., Schwarz, J. P., Moteki, N., Koike, M., Takami, A., and Kondo, Y.: Hygroscopicity of materials internally mixed with black carbon measured in Tokyo, J. Geophys. Res.-Atmos., 121, 362–381, https://doi.org/10.1002/2015jd024153, 2016.

Peng, J., Hu, M., Guo, S., Du, Z., Zheng, J., Shang, D., Zamora, M. L., Zeng, L., Shao, M., Wu, Y.-S., Zheng, J., Wang, Y., Glen, C. R., Collins, D. R., Molina, M. J., and Zhang, R.: Markedly enhanced absorption and direct radiative forcing of black carbon under polluted urban environments, P. Natl. Acad. Sci. USA, 113, 4266–4271, https://doi.org/10.1073/pnas.1602310113, 2016.

Petzold, A., Ogren, J. A., Fiebig, M., Laj, P., Li, S.-M., Baltensperger, U., Holzer-Popp, T., Kinne, S., Pappalardo, G., Sugimoto, N., Wehrli, C., Wiedensohler, A., and Zhang, X.-Y.: Recommendations for reporting "black carbon" measurements, Atmos. Chem. Phys., 13, 8365–8379, https://doi.org/10.5194/acp-13-8365-2013, 2013.

Popovicheva, O., Persiantseva, N. M., Shonija, N. K., DeMott, P., Koehler, K., Petters, M., Kreidenweis, S., Tishkova, V., Demirdjian, B., and Suzanne, J.: Water interaction with hydrophobic and hydrophilic soot particles, Phys. Chem. Chem. Phys., 10, 2332–2344, https://doi.org/10.1039/b718944n, 2008.

Popovicheva, O. B., Kireeva, E. D., Timofeev, M. A., Shonija, N. K., and Mogil'nikov, V. P.: Carbonaceous aerosols of aviation and shipping emissions, Izv. Atmos. Ocean. Phys., 46, 339–346, https://doi.org/10.1134/s0001433810030072, 2010.

Pratt, K. A., Murphy, S. M., Subramanian, R., DeMott, P. J., Kok, G. L., Campos, T., Rogers, D. C., Prenni, A. J., Heymsfield, A. J., Seinfeld, J. H., and Prather, K. A.: Flight-based chemical characterization of biomass burning aerosols within two prescribed burn smoke plumes, Atmos. Chem. Phys., 11, 12549–12565, https://doi.org/10.5194/acp-11-12549-2011, 2011.

Qiu, C., Khalizov, A. F., and Zhang, R.: Soot Aging from OH-Initiated Oxidation of Toluene, Environ. Sci. Technol., 46, 9464–9472, https://doi.org/10.1021/es301883y, 2012.

Ramanathan, V. and Carmichael, G.: Global and regional climate changes due to black carbon, Nat. Geosci., 1, 221–227, https://doi.org/10.1038/ngeo156, 2008.

Sadezky, A., Muckenhuber, H., Grothe, H., Niessner, R., and Poschl, U.: Raman micro spectroscopy of soot and related carbonaceous materials: Spectral analysis and structural information, Carbon, 43, 1731–1742, https://doi.org/10.1016/j.carbon.2005.02.018, 2005.

Schwan, J., Ulrich, S., Batori, V., Ehrhardt, H., and Silva, S. R. P.: Raman spectroscopy on amorphous carbon films, J. Appl. Phys., 80, 440–447, https://doi.org/10.1063/1.362745, 1996.

Semeniuk, T. A., Wise, M. E., Martin, S. T., Russell, L. M., and Buseck, P. R.: Hygroscopic behavior of aerosol particles from biomass fires using environmental transmission electron microscopy, J. Atmos. Chem., 56, 259–273, https://doi.org/10.1007/s10874-006-9055-5, 2007.

Shiraiwa, M., Kondo, Y., Moteki, N., Takegawa, N., Miyazaki, Y., and Blake, D. R.: Evolution of mixing state of black carbon in polluted air from Tokyo, Geophys. Res. Lett., 34, L16803, https://doi.org/10.1029/2007gl029819, 2007.

Sze, S. K., Siddique, N., Sloan, J. J., and Escribano, R.: Raman spectroscopic characterization of carbonaceous aerosols, Atmos. Environ., 35, 561–568, https://doi.org/10.1016/s1352-2310(00)00325-3, 2001.

Tang, M., Cziczo, D. J., and Grassian, V. H.: Interactions of Water with Mineral Dust Aerosol: Water Adsorption, Hygroscopicity, Cloud Condensation, and Ice Nucleation, Chem. Rev., 116, 4205–4259, https://doi.org/10.1021/acs.chemrev.5b00529, 2016.

Tritscher, T., Juranyi, Z., Martin, M., Chirico, R., Gysel, M., Heringa, M. F., DeCarlo, P. F., Sierau, B., Prevot, A. S. H., Weingartner, E., and Baltensperger, U.: Changes of hygroscopicity and morphology during ageing of diesel soot, Environ. Res. Lett., 6, 034026, https://doi.org/10.1088/1748-9326/6/3/034026, 2011.

Vartapetyan, R. S. and Voloshchuk, A. M.: Adsorption mechanism of water molecules on carbon adsorbents, Uspekhi Khimii, 64, 1055–1072, 1995.

Weingartner, E., Burtscher, H., and Baltensperger, U.: Hygroscopic properties of carbon and diesel soot particles, Atmos. Environ., 31, 2311–2327, https://doi.org/10.1016/s1352-2310(97)00023-x, 1997.

Wyslouzil, B. E., Carleton, K. L., Sonnenfroh, D. M., Rawlins, W. T., and Arnold, S.: Observation of Hydration of Single, Modified Carbon Aerosols, Geophys. Res. Lett., 21, 2107–2110, https://doi.org/10.1029/94gl01588, 1994.

Zhang, F., Peng, J., Chen, L., Collins, D., Li, Y., Jiang, S., Liu, J., and Zhang, R.: The effect of black carbon aging from NO_2 oxidation of SO_2 on its morphology, optical and hygroscopic properties, Environ. Res., 212, 113238, https://doi.org/10.1016/j.envres.2022.113238, 2022a.

Zhang, P., Chen, T., Ma, Q., Chu, B., Wang, Y., Mu, Y., Yu, Y., and He, H.: Diesel soot photooxidation enhances the heterogeneous formation of H_2SO_4, Nat. Commun., 13, 5364, https://doi.org/10.1038/s41467-022-33120-3, 2022b.

Zhang, R., Khalizov, A. F., Pagels, J., Zhang, D., Xue, H., and McMurry, P. H.: Variability in morphology, hygroscopicity, and optical properties of soot aerosols during atmospheric processing, P. Natl. Acad. Sci. USA, 105, 10291–10296, https://doi.org/10.1073/pnas.0804860105, 2008.

Zhao, Y., Liu, Y., Ma, J., Ma, Q., and He, H.: Heterogeneous reaction of SO_2 with soot: The roles of relative humidity and surface composition of soot in surface sulfate formation, Atmos. Environ., 152, 465–476, https://doi.org/10.1016/j.atmosenv.2017.01.005, 2017.